Rare Metal Materials and Engineering
Volume 52, Issue 8, August 2023
Available online at www.rmme.ac.cn

Science Press

Cite this article as: Xu Kai, Wang Mingqiu, Fang Naiwen, et al. Effect of Heat Treatment on Microstructure and Properties of Titanium Alloy Welded Joint by Laser Welding with Flux-Cored Wire[J]. Rare Metal Materials and Engineering, 2023, 52(08): 2665-2675.

ARTICLE

Effect of Heat Treatment on Microstructure and Properties of Titanium Alloy Welded Joint by Laser Welding with Flux-Cored Wire

Xu Kai[1], Wang Mingqiu[2], Fang Naiwen[1], Wu Pengbo[1], Huang Ruisheng[1], Sun Laibo[1], Li Wei[3], Wang Xingxing[4], Zhou Zhenzhen[1], Li Shuai[4], Zhang Tianli[5]

[1] Harbin Welding Institute Co., Ltd, Harbin 150028, China; [2] Shanghai Zhongxun Technology Co., Ltd, Shanghai 200120, China; [3] Beijing Jinwei Welding Material Co., Ltd, Tianjin 301906, China; [4] Henan International Joint Laboratory of High-Efficiency Special Green Welding, North China University of Water Resources and Electric Power, Zhengzhou 450045, China; [5] School of Materials Science and Engineering, Shanghai University of Engineering Science, Shanghai 201620, China

Abstract: Ti-6Al-4V titanium alloy plate was welded by a laser beam with self-developed titanium alloy flux-cored wire. The welded joint was solution treated at 920 °C for 1 h and aging treated at 650 °C for 2 h, and its microstructure and properties were compared with those of the as-welded joint. The results show that the heat-treated welded joint is composed of a typical tri-modal microstructure containing α_p phase, α_s phase colony, and α_{gb} phase, as well as punctate distributed residue β phase. α' martensite microstructure in the as-welded joint is not found in the heat-treated joint, which makes the strength, plasticity, and toughness well balanced and maintained. The strength of the heat-treated welded joint is reduced, while elongation and impact toughness at room temperature are enhanced. The tensile fracture of the heat-treated welded joint is surrounded by massive shear lips. The dimples are deep and uniform, presenting as microvoid coalescence ductile fracture. In the as-welded joint, the proportion of large-angle grain boundaries with misorientation between grains in the weld zone greater than 15° accounts for 83.78%, and in the heat-treated welded joint, the proportion is about 90.21%. Through XRD test, it is discovered that the as-welded weld is mainly composed of α' martensite, with a small amount of extremely weak multi-angle α phase diffraction peak. In the heat-treated weld, the central angle position of α phase diffraction peak is consistent with that of α' martensite in the as-welded weld, with a sharp β phase (110) diffraction peak observed as well.

Key words: titanium alloy; laser welding with filler wire; heat treatment; microstructure and mechanical properties

Ultra-strong alloys with high ductility are critical for facing the challenges in lightweight development. Therefore, titanium alloys with high specific strength have become the most widely used metal materials in aerospace and military industries. With low density, high specific strength, good corrosion resistance, and fatigue resistance, titanium alloys have been widely utilized in the weaponry and marine industry[1–2]. As a typical α-β dual-phase titanium alloy having both the advantages of α type and β type titanium alloys[3], Ti-6Al-4V is the most widely used alloys among titanium alloys. Compared with traditional welding technologies, narrow gap laser welding with filler wire has advantages such as small heat input, narrow heat affected zone, high welding efficiency. Meanwhile, the use of filler wire helps to supplement burnt alloys and beneficial alloy elements, thus further optimizing the microstructure and properties of the welded joint. Therefore, it has gained extensive attention in titanium alloy welding[4–5].

Narrow gap laser welding with filler wire is a process of heat accumulation of single-pass multi-layer filler metal. In the welding process, several times of thermal cycles occur, which generates highly complex and non-uniform weld microstructure, resulting in uneven distribution of stress and deformation in the welded joint, affecting the safety

Received date: February 04, 2023
Foundation item: National Key Research and Development Plan of China (2021YFB3401100); Heilongjiang Head Goose Action Plan-Advanced Welding Technology Innovation Team of Energy Equipment (201916120); Open Project of the State Key Laboratory of New Brazing Materials and Technology (SKLABFMT202005)
Corresponding author: Fang Naiwen, Ph. D., Professor, Harbin Welding Institute Co., Ltd, Harbin 150028, P. R. China, Tel: 0086-451-86312374, E-mail: fangnw@hwi.com.cn

performance of titanium alloy welding parts, and thus limiting the application in industrial manufacturing[6–7]. The thermal conductivity of titanium alloy is poor. In laser high-energy beam welding, the titanium alloy molten pool temperature is high, providing a sufficient conditions for the growth of the high-temperature β phase. During the rapid cooling process after welding, diffusionless displacive transformation ($\beta \rightarrow \alpha'$) occurs, and high-density heterophase boundaries (PBs) are introduced to the titanium alloy weld microstructure. With α' martensite phase transformation in titanium alloy weld microstructure, interface hardening is generated by the build-up of dual-phase microstructure through rapid cooling-driven phase transformation. At the same time, hardening is generated by stress-induced phase transformation. Generally, the yield strength of the weld tends to be lower, and work hardening ability and fracture elongation are enhanced. Therefore, relevant researchers tried to optimize the mechanical properties by adjusting the density and spatial distribution characteristics of grain boundaries (GBs) and heterophase boundaries (PBs)[8]. It is found that the comprehensive mechanical properties of the titanium alloy welded joint can be significantly improved by controlling the interface structure and features of α/β phases with discontinuous lattice. The existence of relatively large β grains with tens or even hundreds of microns in size in the titanium alloy welded joint usually leads to the formation of micron and submicron α' lamella, resulting in low phase interface density and poor joint plasticity. Therefore, it is still a challenge to construct high-strength, and high-toughness titanium alloy welded joint with fine structures using grain boundary engineering (GBE). Heat treatment has become an appropriate method to further regulate the composition, morphology, and distribution of weld microstructure and to optimize the welded joint's comprehensive mechanical properties.

The titanium alloy microstructure is sensitive to the heat treatment process. Through heat treatment, the microstructure of the titanium alloy welded joint is changed, and the microstructure distribution of each zone of the welded joint is coordinated, so uniformity of stress and deformation of the welded joint are improved. In recent years, scholars have researched the heat treatment of titanium alloy welded joints and plates. Yu et al[9] adopted vacuum electron beam welding to join a Ti55531 titanium alloy plate with 60 mm in thickness and obtained full penetration welded joint. The results showed that solution treatment can reduce the microhardness of different zones of the joints and improve impact toughness, and the tensile strength of the welded joint can be increased to 1129 MPa. Lei et al[10] studied the effect of aging heat treatment on microstructure and phase transformation of laser oscillating welded TB8 titanium alloy joints and established a correlation between tensile properties and microstructure. It is found that the segregation of major alloy elements such as Al, Mo, and Nb is the main reason for the poor- and rich-precipitation zone in the weld area. Low-temperature aging deteriorates the plasticity of welded joints, while high-temperature aging improves the ambient- or elevated-temperature tensile properties of joints. The influence of aging temperature and aging time on the microstructure evolution was also discussed. After aging treatment at 450 °C for 1 h, the intermediate ω phase in the gathering place is transformed to α phase, and the dispersed ω phase is still retained. With the increase in aging temperature and time, the size of α phase precipitate increases. It is also discovered that the tensile strength is increased by 85% after high-temperature aging treatment, and Portevin-Le Chatelier (PLC) effect can be avoided under thermos-mechanical loading conditions. Guo et al[11] conducted heat treatment on linear friction welded joint of Ti6246 alloy at 600 °C for 1 h. It was found that the microstructure of the as-welded weld zone is composed of fine grains with dense acicular α''. After heat treatment, the microstructure of the weld zone is transformed from α'' to α. Wu et al[12] explored the microstructure evolution, mechanical properties, and fracture mechanism of Ti-5Al-5Mo-5V-3Cr-1Zr titanium alloy plate under different solution and aging heat treatment conditions. It can be seen from the results that the volume fraction of the primary α_p phase decreases with increasing solution temperature, and the length of the secondary α_s phase is reduced while its width increases with raising solution temperature. The yield strength and tensile strength of Ti-5Al-5Mo-5V-3Cr-1Zr titanium alloy plate decrease with the increase in solution temperature but enhance with the increase in aging temperature. The tensile strength and toughness of the alloy obtained under the conditions of solution at 800 °C for 2 h and aging at 640 °C for 8 h are optimal. With the increase in aging temperature and time, the secondary α_s phase becomes coarsened, which makes the microcrack propagation path tortuous and deflected, thus increasing the crack propagation resistance and ultimately improving the fracture toughness of the alloy.

There are few slip systems of HCP phases in Ti-6Al-4V dual phase titanium alloy joint welded by laser welding with filler wire. With strong anisotropy, the crystal structure features of the joint determines its poor plasticity. Therefore, the key of property regulation of the Ti-6Al-4V dual-phase titanium alloy welded joint is to enhance its plasticity and toughness through heat treatment.

By referring to a large number of relevant literatures, it is found that with the development and design of titanium alloy flux-cored wire, there is little research on the regulation of the grain size, orientation and distribution of weld by the addition of beneficial elements and the supplement of burning element in the welding process. Therefore, the research group carried out the development and design of titanium alloy flux-cored wire in the early stage, and analyzed the microstructure and properties of the obtained welded joints. It is found that the grain refinement of weld microstructure is obvious, and the performance is also greatly improved. Based on the previous research, a self-developed Ti-Al-V flux-cored wire was used as the filler metal in the present research. Solution and aging treatment were conducted on the obtained welded joint, which was then compared with the as-welded joint for its microstructure, properties, and phase composition. The

present study is expected to provide technical support for the heat treatment process and control and regulation of microstructure and properties of laser welded joints of titanium alloys.

1 Experiment

The size of Ti-6Al-4V titanium alloy plates used in the experiment was 400 mm×200 mm×20 mm. The filler metal was Ti-Al-V flux-cored wire with a diameter of 1.6 mm. The chemical composition of the base metal and deposited metal is shown in Table 1. The test plates to be welded were first processed into a Y-shape groove, with a root face of 2 mm, a root opening of 3.2 mm, and a bevel angle of 1.5°. Before welding, the test plates were polished and pickled in a solution with 5vol% HF+30vol% HNO_3+H_2O. After removing the oil strain and oxide from the plate surface, the acid solution remaining on the plates was cleaned with alcohol and water, and then the plates were dried. Laser welding with filler wire was adopted for the filling of grooves in the test plates. The welding heat input was provided by IPG's YLS-6000 fiber laser. A Fronius KD 1500 D-11 wire feeder and a KUKA robot were used to control the welding trajectory through a cantilever gantry-integrated welding system.

The laser beam adopted the circular oscillation mode with an oscillating frequency of 100 Hz and an amplitude of 2 mm. Other welding parameters are shown in Table 2. A single laser was used in backing welding, and 6 layers in total were filled. The interlayer temperature was controlled at 150±15 °C. Ar was used as the shielding gas to protect both sides (front and back) of the weld during the welding process. The output pressure was 0.5 MPa. Two titanium alloy plates were laser welded with filler wire using the same parameters.

After welding, one of the test plates was held at 920 °C for 1 h and then air cooled to room temperature. It was then heated to 650 °C and held for 2 h, followed by air-cooling to room temperature. One as-welded plate and one heat-treated plate were processed by a wire-cutting machine for sample preparation. Microstructure and phases were observed and analyzed by OLYMPUSGX71 optical microscope, JEM-2100F high resolution field emission transmission electron microscope (FE-TEM), electron backscatter diffractometer (EBSD), FEI Quanta-200 scanning electron microscope and D/MAX-rB X-ray diffractometer. The hardness test was conducted with an HVS-1000Z microhardness tester. The tensile properties at room temperature were tested on INSTRON 5569 electronic universal testing machine.

2 Results

2.1 Microstructure evolution

Fig. 1 shows the overall and cross-sectional macroscopic appearance of Ti-6Al-4V titanium alloy welded joint. Defects such as pores, cracks, and sidewall lack of fusion are not observed. The weld zone of the welded joint is composed of coarse columnar grains, which grow along the temperature gradient increase direction. Columnar grains grow from both sides of the weld to the weld center. In a vertical growth direction, the columnar grains finally meet at the weld center. Under the optical microscope, the electric potential difference between α phase and β phase is different. β phase is easy to corrode and becomes dark, while the α phase is difficult to corrode and becomes bright. It can also be found that the width of the heat affected zone of the welded joint is relatively

Table 1 Chemical composition of base metal and deposited metal (wt%)

Plate	Al	V	Fe	C	N	H	O	Ti
Ti-6Al-4V base material	6.30	4.11	0.018	0.024	0.007	0.001	0.14	Bal.
Ti-Al-V flux cored wire deposited metal	6.10	4.15	0.040	0.012	0.006	0.001	0.02	Bal.

Table 2 Welding parameters

Welding layer	Laser power, P/W	Welding speed, V_1/m·min^{-1}	Wire feed speed, V_2/m·min^{-1}	Focal length, f/mm	Defocus quantity, Δf/mm
Backing welding	3500	1.00	1.5	425	+20
2–7 filling welding	3000	0.65			

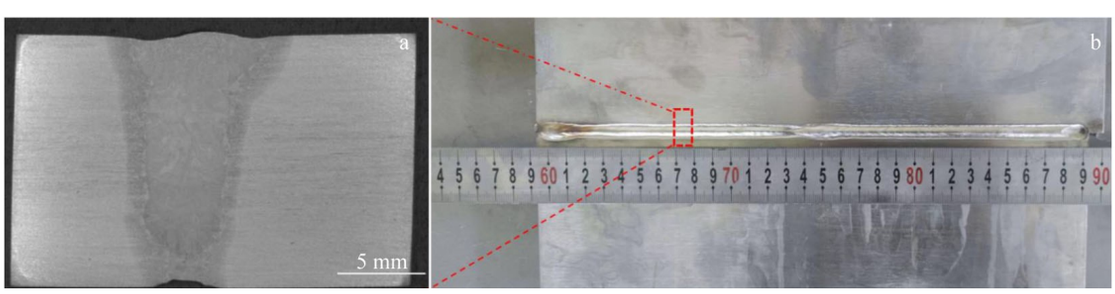

Fig.1 Macroscopic appearance of welded joint

narrow, about 1 mm.

Fig. 2 is the microstructure morphology of the as-welded joint. It can be found that the largest grain microstructure appears in the weld zone. As their distance from the weld increases, the grains decrease gradually in dimension. That is, the size of grains in the weld zone, heat affected zone, and base metal decreases gradually. Fig.2d and Fig.2g are the OM and SEM images of the WM zone. It can be found that there are a lot of columnar grains in the weld, and the weld interior is basketweave microstructure interwoven by acicular α' martensite. During the rapid solidification process of the molten pool, alloy elements have no time to diffuse and thus shear to form a supersaturated α' martensite solid solution. α' martensite grows and nucleates inside the original β columnar grains, first forming one or several paralleled primary α' martensite, which extend through the whole grain and stop at grain boundaries. Then there are a series of relatively fine secondary acicular α' martensite, which stops extension at grain boundaries or when meeting primary α' martensite. This leads to the final basketweave morphology of the weld zone, which is full of acicular α' martensite. Fig. 2c and Fig. 2f are the OM and SEM images of the heat affected zone. The zone consists of a few primary α_p phases, Widmanstatten structure, and α' martensite, which are induced by the rapid cooling of the metal near the weld during welding after being heated to a higher temperature. The quantity of acicular α' martensite in this zone is less than that of the weld, and the size is finer. Due to different distances between each part of the heat affected zone and the melt pool, the influence is various. Grains near the fusion line are coarser and bigger than those far from the fusion line, and acicular α' martensite near the fusion line tends to be denser and more numerous. The fusion line shows the characteristics of epitaxial solidification of columnar grains and equiaxed grains. Fig. 2b and Fig. 2e present the OM and SEM images of the base metal. In the base metal, bimodal morphology, composed of interlaced equiaxed and elongated α phase and β phase, can be observed. Moreover, a small amount of secondary α_s phase can also be found in the β phase.

Fig. 3 shows the microstructure morphology of the welded joint after heat treatment. It is noted that the composition and morphology of the microstructure are pretty different from those of the as-welded joint. Fig. 3d and Fig. 3g are the OM and SEM images of the WM. The primary α_p phase undergoes incomplete recovery during heat treatment, and grains appear to be equiaxed. The microstructure is composed of secondary α_s, grain boundary α_{gb} phase, and β phase. Fig. 3c and Fig. 3f are the OM and SEM images of the heat affected zone. It can be noted that the original β phase boundaries are no longer clearly visible, and the microstructure is mainly composed of finer secondary α_s phases, grain boundary α_{gb}, and a few residue β phases, with widmanstantten structure disappearing at the same time. Fig. 3b and Fig. 3e are the OM and SEM images of the base metal. In addition to the bimodal morphology, the base metal, after heat treatment, is also found with increased equiaxed α phase and finer β and reduced content. Moreover, no secondary α_s phase is detected. The microscale of each zone of the two groups of welded joints is also clearly distinctive. The thickness of the lamellar structure and width of the original β phase grain boundary of each zone

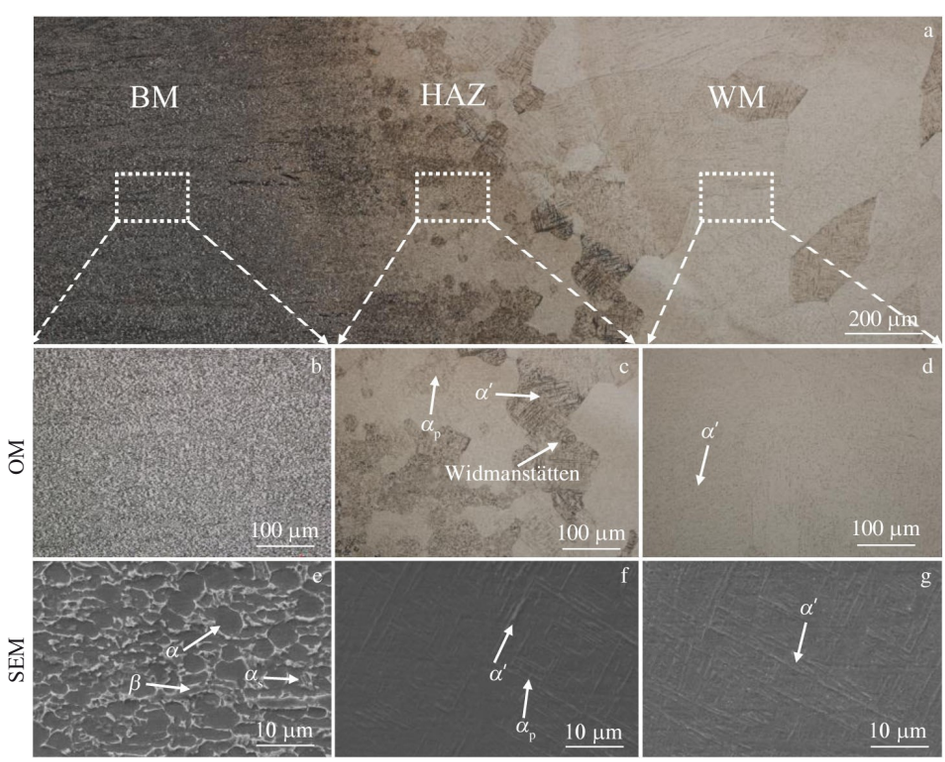

Fig.2 Microstructures of welded joint without heat treatment: (a) overall micromorphology, (b, e) BM, (c, f) HAZ, and (d, g) WM

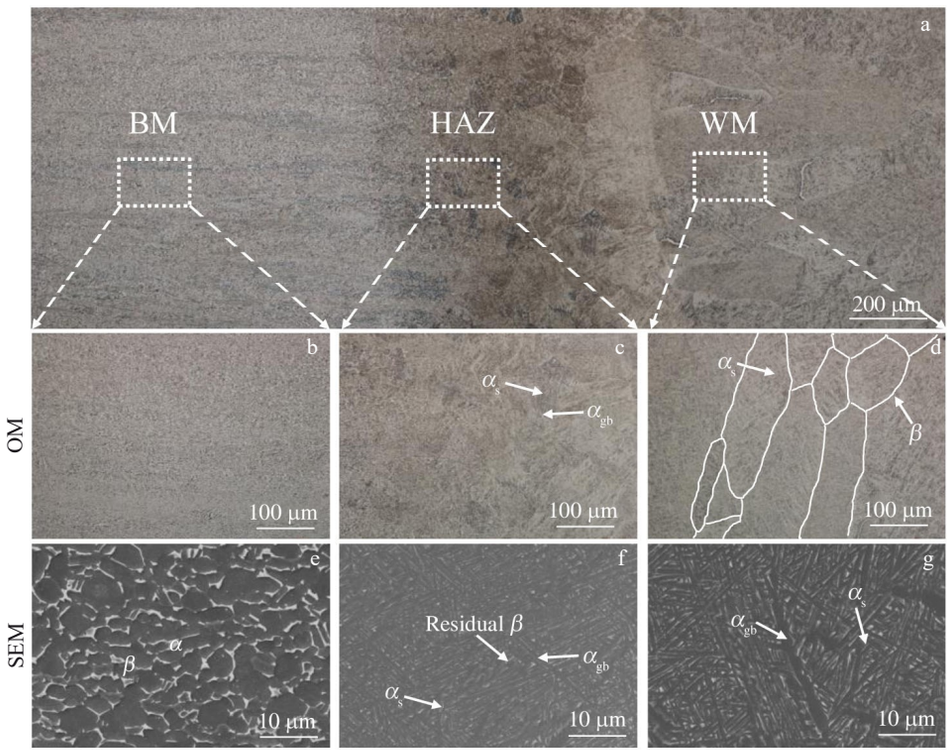

Fig.3 Microstructures of welded joint with heat treatment: (a) overall micromorphology, (b, e) BM, (c, f) HAZ, and (d, g) WM

in the heat-treated welded joint increase obviously, and the thickness of the lamellar α phase is increased to a certain extent. It is due to the rapid air cooling of the near β phase in the first stage retaining crystal defects in the microstructure, which provides abundant nuclei for the lamellar α phase nucleation. The precipitation of the lamellar α phase is essentially nucleation and growth processes. Generally, the secondary lamellar α_s phase nucleates at β phase grain boundary. Due to the specific orientation relationship, the secondary lamellar α_s phase grows rapidly in the length direction after its nucleation and stops the growth at β grain boundary or phase interface. Then the thickness of the lamellar α phase and the size of the primary α phase begin to increase. Due to the transformation from β to α, the volume fraction of the equiaxed primary α_p phase slightly increases. Because of the second annealing, alloy elements in the lamellar α phase diffuse more violently with the increase in temperature. After the nucleation and growth of the lamellar α phase, there is enough time for its coarsening, and its thickness also increases.

Fig.4 shows the TEM image of the weld zone of two groups of welded joints. Fig.4a and Fig.4b are TEM morphologies of the weld zone of the as-welded joint under low and high magnifications. In Fig.4a, the average width of α' martensite lath is about 0.35 μm. There are a few residue β phases interspersed among lath α' martensite. Relatively dense locations can be found in α' martensite because when β phases shear to α' martensite in the cooling process of high temperature β zone, Burgers orientation relationship is followed, resulting in the occurrence of dislocation to coordinate the strain generated during the phase transformation [13–14]. A relatively dense dislocation block can be observed inside α' martensite in Fig.4b, and Fig.4c–4d are TEM morphologies of the weld zone of the heat-treated joint under both low and high magnifications. In Fig.4c, the width of the finally formed lath α phase is obviously increased, with an average width of about 0.95 μm. It can be found that the dislocation density in the weld after treatment is greatly reduced. According to the research of Zuo[15] and Castany et al[16], dislocations usually first appear at phase boundaries. Therefore, dislocation density at the phase boundaries is significantly higher than that inside the phase. At the same time, it is found in Fig. 4d that a dense dislocation wall is formed at α/β boundaries, which is related to the thermal expansion coefficient of α phase and β phase. The thermal expansion coefficient of the α phase is much lower than that of the β phase. Therefore, the greater thermal stress is inevitably concentrated at α/β boundaries, leading to dense dislocation in corresponding areas.

Fig. 5 is the grain morphology and orientation of the weld zone of the two groups of welded joints. Fig.5a and Fig.5b are the images of the as-welded joints. Fig. 5c and Fig. 5d are the images of the heat-treated joints. Two types of original β phase boundaries are observed, namely continuous grain boundaries and discontinuous ones, which is also verified by Lei[17] and Zafari et al[18] in their research. During the second intermediate temperature annealing process of the heat-treated joint, the cooling speed of the weld zone is high, and the generated supercooling is large, which makes the crystal nucleus occur at grain boundaries and grow into grain

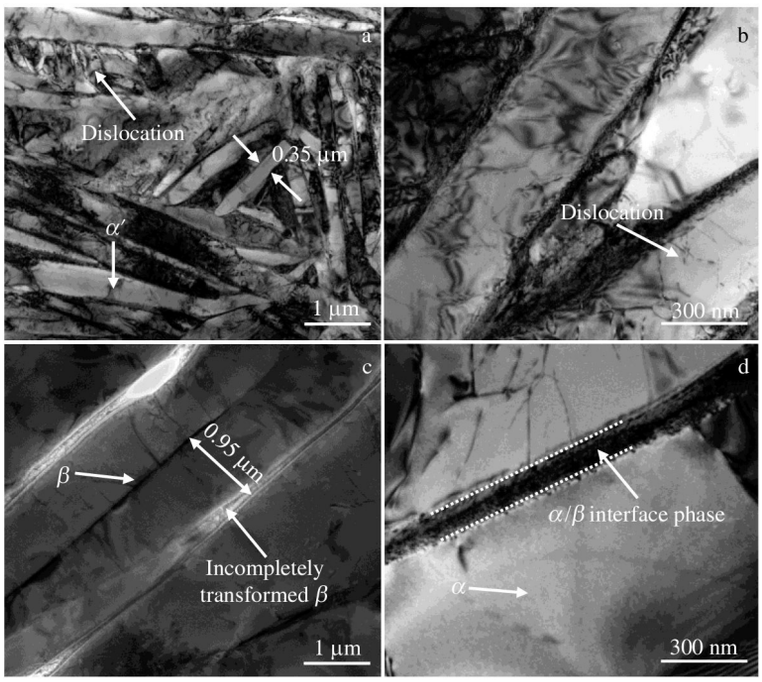

Fig.4 TEM images of welded metal without (a–b) and with (c–d) heat treatment

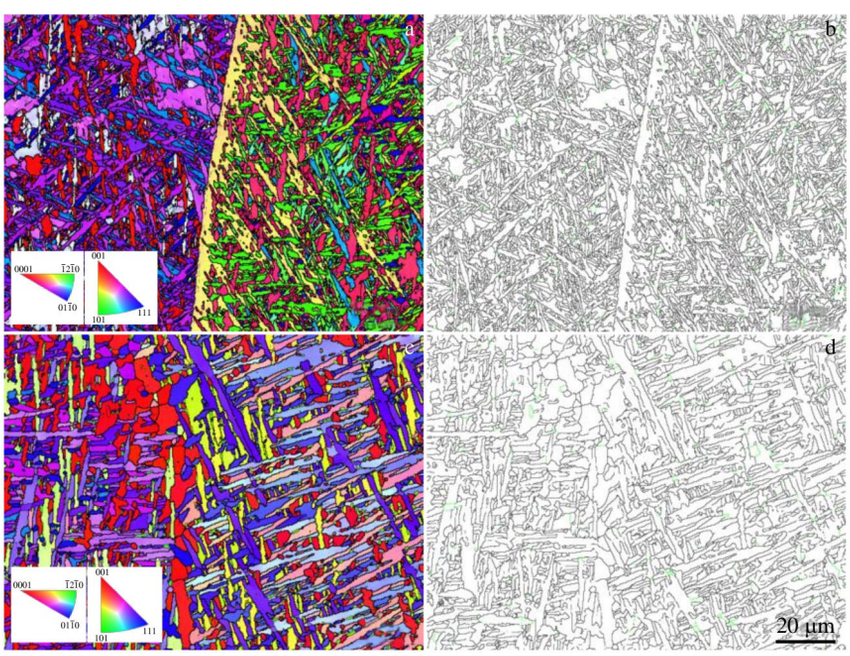

Fig.5 EBSD orientation images of weld seam without (a–b) and with (c–d) heat treatment

boundary α_{gb} phase. At the same time, secondary α_s phases are formed among primary α_p phases to form a disordered basketweave morphology. It explains how discontinuous grain boundaries appear. The direct cooling of β phase high temperature zone gives enough time and nucleation driving force for the primary α_p phase to nucleate and to grow into continuous grain boundaries. Zhang et al[19] proves that inhabiting the generation of continuous grain boundary α_{gb} phase can improve the ductility and toughness of titanium alloys.

Microstructure with different orientations in the two groups of welds is intertwined with each other, which is conducive to inhibiting crack growth and improving the toughness of relevant materials. In comparison, it can be seen that the acicular microstructure in the heat-treated weld zone is finer, and the length-diameter ratio is smaller. The green lines in Fig. 5b and Fig. 5d represent low grain boundaries (2°~15°), and the black lines represent large angle grain boundaries (>15°). It can be seen that the proportion of large-angle grain boundaries in the heat-treated weld zone is slightly higher.

The distribution of misorientation of the two groups of welded joints is shown in Fig.6.

The calculated misorientation distribution of grains in the as-welded zone is shown in Fig.6a. Large grain boundaries (> 15°) account for about 83.78%, and those between 55.5° – 66.5° account for about 73.67%. The misorientation distribution of grains in the heat-treated weld zone is shown in Fig. 6b, of which large grain boundaries (>15°) account for about 90.21%, while grain boundaries between 55.5° – 66.5° account for about 76.05%. According to the descriptions in Ref.[20–21], impact toughness is closely related to the orientation distribution. Misorientation distribution between large-angle grain boundaries can effectively prevent microcracks from expanding in the intragranular microstructure. For low-angle grain boundaries, cracks can propagate only by deflecting a little from the next grain boundary. Therefore, the above test results indicate that the impact toughness of the weld zone of the heat-treated joint is better.

To determine the phase composition of the weld of the two groups of welded joints, XRD was used, as shown in Fig. 7. The weld zone of the two groups of welded joints is mainly composed of hcp crystal structure, and no orthorhombic lattice structure is observed. According to the lattice constant ratio c/a and the above microstructure analysis, it can be determined that the as-welded weld is mainly composed of α' martensite, with strong peaks appearing at 2θ=40.5° . There are also a few weak multi-angle α phase diffraction peaks.

The central angle position of α phase diffraction peak in the heat-treated weld is the same as that of α' martensite in the as-welded weld. The diffraction peak of β phase (110) is sharp and shifts to the right, because in the process of heat treatment, nonequilibrium α' martensite is transformed to β phase and retained in the subsequent furnace cooling process. The rightward shifting of the diffraction peak indicates that the lattice constant of the weld microstructure becomes smaller after heat treatment, and the interplanar spacing also decreases[22]. With the cooling of β phase, α phases nucleate at β phase grain boundaries and grow along a certain orientation inside β phase grains, which indicates that heat treatment increases the solid solubility of the weld.

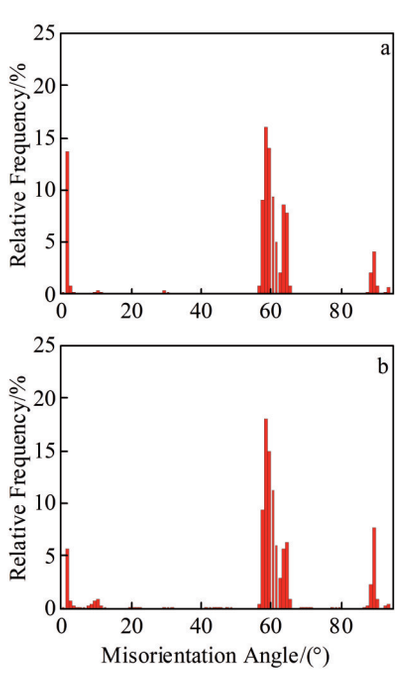

Fig.6 Misorientation angle distribution of welded metal without (a) and with (b) heat treatment

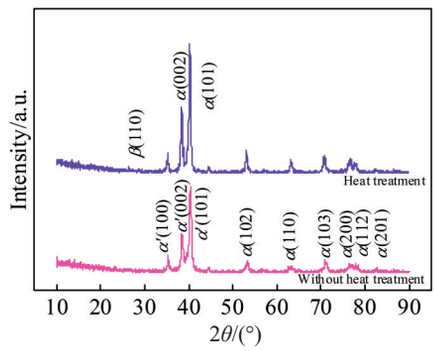

Fig.7 XRD patterns of welded metal

2.2 Mechanical properties

Fig. 8 shows the microhardness distribution of the two groups of welded joints. Overall, the microhardness of each zone ranks as weld zone＞heat affected zone>base metal. The hardness distribution of the welded joints is closely related to their microstructure composition and phase content. There are dislocations and twinning with high density in α' martensite[23], so a considerable number of grain boundaries can be generated. Therefore, its hardness is significantly higher than those of other phases. In the two groups of welded joints, the hardness of the weld zone with the most α' martensite is better than those of the heat affected zone and the base metal.

The hardness values of the corresponding areas of the two groups of welded joints are slightly different. The overall microhardness value of the heat-treated joint is lower than that of the as-welded joint. The reason is that recovery and recrystallization occur in the joint microstructure during heat treatment, and the vacancy concentration of the microstructure reduces, resulting in the formation of the substructure.

In the hardness loading process, the load makes dislocation

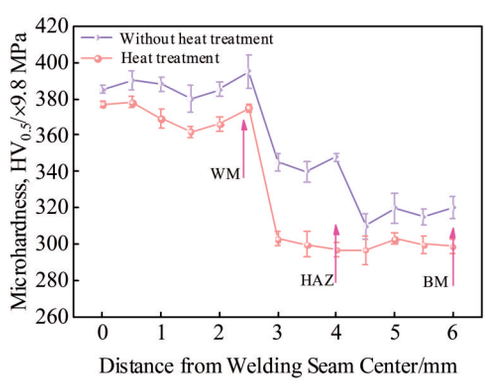

Fig.8 Microhardness distribution of welded joint

slip to grain boundaries, which results in dislocation blocks. Grain boundaries have an obvious blocking effect on dislocation motion. As the load increases, the density of dislocation blocks increases, accompanied by the generation of stress concentration. When the concentrated stress is big enough to overcome the blocking effect of the grain boundaries, stress releases and plastic deformation occurs, which leads to the dislocation motion of the adjacent grain microstructures, and the occurrence of the intersection of grain boundaries in adjacent grain microstructures to harden the material [24]. As heat treatment can reduce dislocation density [25], the dislocation density in the weld zone and heat affected zone of the heat-treated joint is lower than that in the corresponding zones of the as-welded joint, resulting in lower hardness of the heat-treated joint.

Table 3 shows the result of the tensile test at room temperature and impact properties for TC4 titanium alloy base metal and the two groups of welded joints. The tensile strength of the heat-treated welded joint is slightly lower, while the elongation and impact properties at room temperature are greater than those of the as-welded joint and base metal. By comparing the results of TC4 titanium alloy laser wire filling welding conducted by relevant scholars [26–27] using solid welding wire, it can be seen that the welded joints in both welding state and heat treatment state have obvious advantages in tensile properties and impact properties.

Fig. 9 shows the microstructure under low magnification and the microstructure of selected areas under high magnification of the two groups of tensile specimens after fracturing at room temperature. Fig. 9a–9c show the macroscopic and microscopic morphologies of tensile specimens of the as-welded joint after a fracture. The fracture surface is

Table 3 Tensile and impact properties of titanium alloy base metal and welded joints

Inspection item	Tensile strength, R_m/MPa	Elongation percentage, A/%	Fracture location	Impact toughness at room temperature, KV_2/J
Base metal	925	12.5	-	20
Welded joint without heat treatment	928	13.0	BM	12
Welded joint with heat treatment	923	14.0	WM	16

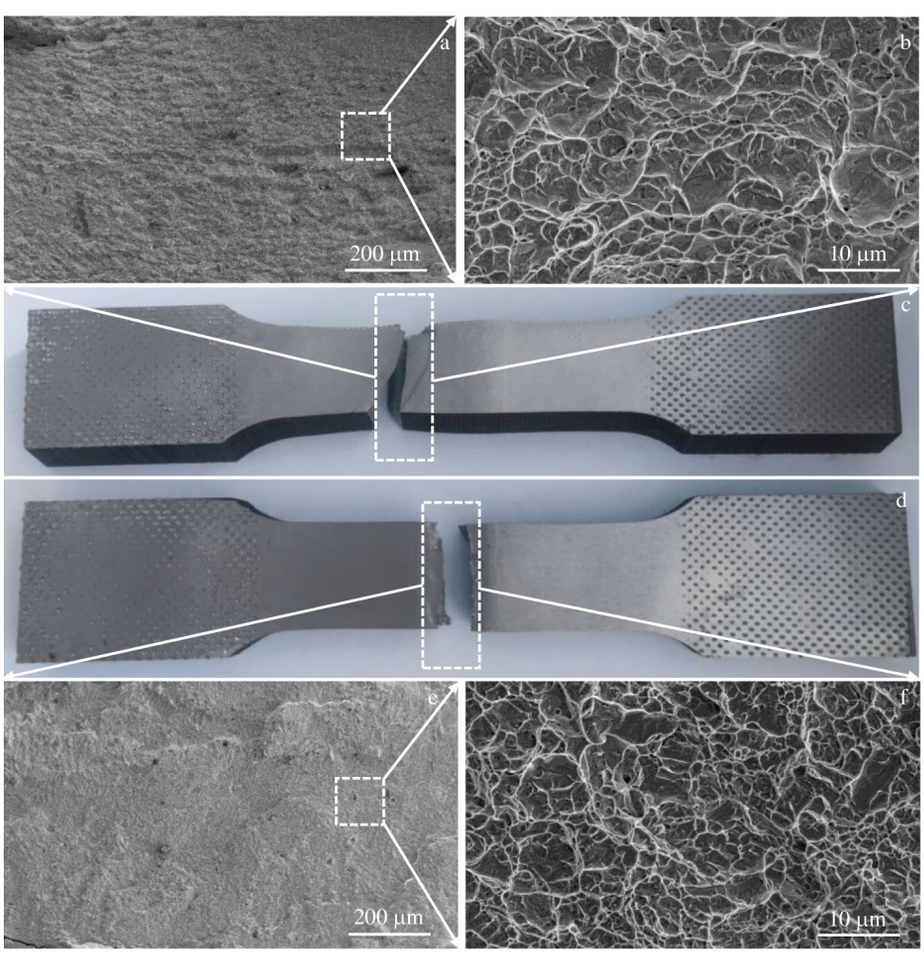

Fig.9 Microstructures and morphologies of tensile specimens after fracture: (a–c) without heat treatment and (d–f) with heat treatment

relatively flat, and the dimples are shallow with different sizes. Fig. 9d – 9f are the fracture morphologies of impact specimens of the heat-treated joint. The dimples are deep and uniformly distributed.

After annealing for the welded joint, the original Widmanstatten structure in the weld transforms to α phase basketweave microstructure, and grain boundaries are broken or even disappear. Therefore, the inhibiting effect of grain boundaries on slipping is weakened, leading to the increase in slipping distance and significantly improving the plasticity [28]. At the same time, α' martensite with higher strength transforms to coarse $\alpha+\beta$ phase, leading to the reduction in tensile strength. In addition, the interlaced coarse lamellar structure and fine lamellar structure in a single α' martensite cluster cause the deviation of crack propagation direction, which has an obvious blocking effect on the crack propagation and is conducive to improving weld plasticity [29].

Fig. 10 is the macroscopic and microscopic fracture morphologies of impact specimens at room temperature. Fig. 10a and Fig. 10c are the fracture images of the as-welded joint. River-like fracture, which is a cleavage fracture, is clearly visible. The toughness of the fracture is poor. Fig. 10b and Fig. 10d are the fracture images of the heat-treated joint. Shear lip and ductile fracture features are found in the fracture, and good impact toughness is obtained. From the enlarged image of the selected area in Fig. 10c, it can be found that the fracture of the crack initiation region of the specimens is mainly composed of tearing dimples, and holes can be found simultaneously. The enlarged image in Fig. 10d shows that the fracture of the crack initiation region of the specimens is composed of shear dimples. The crack initiation region of the impact fracture of the heat-treated joint is wider than that of the as-welded joint. The number of holes is greatly reduced. After heat treatment, the lamella thickness of the secondary α_s phase in weld microstructure increases, which hinders crack propagation during the fracture process and thus makes the propagation path tortuous. Therefore, the fracture of the specimens is uneven in morphology.

Relevant scholars [30] proved that impact toughness is closely related to the thickness of the lamellar structure. Weld microstructure after annealing consists mainly of α_s phase lamellar structure with larger lamellar thickness. There are a few punctuate-distributed β phases and grain boundary α_{gb} phases. During the impact process of the specimens, the deflection is easy to occur in the crack propagation direction of the coarse and fine lamella and at α/β interface, leading to a tortuous propagation path and impact toughness improvement. The welded joint is heated to 920 °C for heat preservation. In the subsequent cooling process, metastable phases are induced to form and to decompose. A lot of metastable phases are used as nucleation particles of the α phase, resulting in the increase in nucleation rate of the α phase. The precipitation of massive fine secondary α_s phases truncates primary α_p phase lath so that the length-width ratio of α phase lath decreases. Meanwhile, with the increase in secondary α_s phase content, more segmentation occurs in the grains. These segmentations reduce the cross-slip frequency of dislocations [31] and increase the tolerance of dislocations in the grains, thus improving the impact toughness of the welded joints.

3 Discussion

In order to study the influence of microstructure on impact toughness, Mehdi et al[32] conducted TIG welding for TC4 titanium alloy and obtained the relationship between impact toughness and microstructure parameters. The results show that impact toughness is determined by anti-critical crack nucleation capacity and crack propagation capacity, that is:

$$C_v=C_{vi}+C_{vp} \quad (1)$$

where C_v is the total impact energy, C_{vi} represents the crack formation energy, and C_{vp} is the sum of unstable propagation energy and shear lip formation energy. Through analysis, it is found that the morphology of the α phase has a significant influence on impact toughness. Primary phase α_p is a channel for crack initiation and propagation, and the toughness of the material improves with the increase in the mean free path of

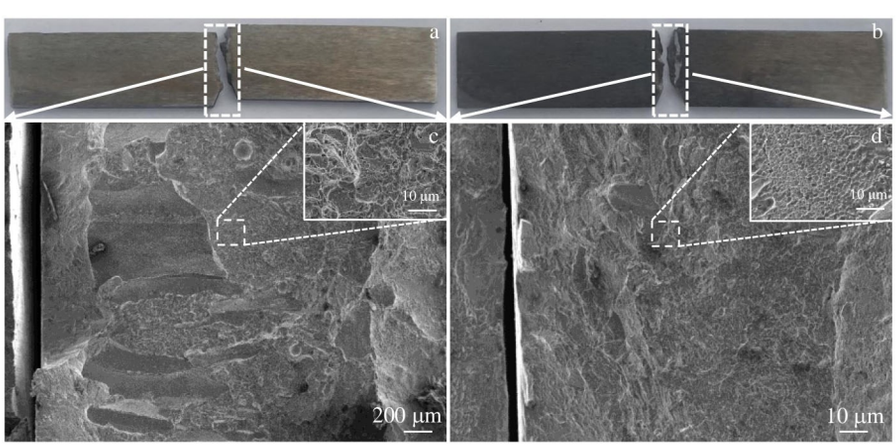

Fig.10 Microstructures and morphologies of impact specimens after fracture: (a, c) welded joint without heat treatment and (b, d) welded joint with heat treatment

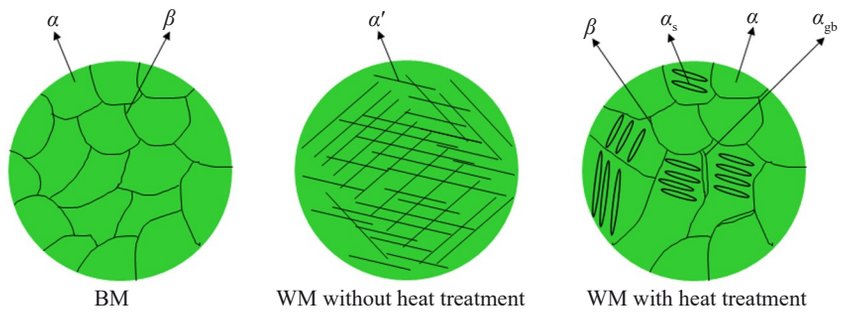

Fig.11 Microstructure evolution during heat treatment

the α_p phase. The morphology of secondary α_s phase is a short rod-like ductile phase. When meeting with cracks, plastic deformation occurs, so more energy is absorbed, and good impact toughness is gained. It is also found that the increase in α' martensite can reduce the impact toughness because of the massive dislocations inside α' martensite. As for the influence of microstructure on impact toughness, the research of Chen et al[33] showed that cracks are easy to occur at grain boundaries of the primary α_p phase, α/β interface, and grain boundaries of β phase. As for the basketweave microstructure, due to its cross-shaped α phase lamellar structure, its crack propagation path is more tortuous with more energy absorbed, showing good impact toughness. In conclusion, for the weld microstructure of $\alpha+\beta$ dual phase titanium alloy, the impact toughness of the lamellar structure with a moderate size is better than that of the equiaxed and bimodal structures. Therefore, in practical applications in the future, the lamellar structure with moderate size can be obtained by heat treatment to obtain excellent impact properties.

During heat treatment, acicular microstructure transforms to lamellar microstructure in the weld of laser welded Ti-6Al-4V titanium alloy with filler wire, as shown in Fig.11. Firstly, by using laser welding with filler wire, in Ti-6Al-4V titanium alloy base metal, equiaxed α phase and β phase directly shear to acicular α' martensite during the cooling process, presenting basketweave distribution. In the subsequent heat treatment process, supersaturated alloy elements in α' martensite diffuse outward, resulting in the transformation of acicular α' martensite in the original weld to α phases and a few β phases. Under the action of internal stress, the lamella of the α phase breaks, thus forming trimodal microstructure mixed with the secondary α_s phase of the short lamella, equiaxed α phase, and α_{gb} phase. There is no fixed orientation relationship in the same matrix of a few equiaxed α phases, and dislocations are easy to find movable slip plane, which plays a coordinating role in deformation. The lamellar secondary α_s phase reduces the mean free path between equiaxed α phases, thus narrowing slip band spacing. The dislocation lines are uniformly distributed, and there are no serious blocks of local dislocations, thus delaying the nucleation and expansion of holes, and realizing the balance between weld strength, plasticity, and toughness.

4 Conclusions

1) The microscale of each zone of as-welded and heat-treated joints is distinctive. The heat-treated weld zone is composed of the secondary α_s phase, grain boundary α_{gb} phase, and β phase, and no α' martensite is observed. The heat affected zone is composed of finer and smaller secondary α_s phases, grain boundary α_{gb} phase, and a few residue β phases, and the widmannstatten structure disappears. Trimodal microstructures mixed with secondary α_s of the short lamella, equiaxed α phase, and α_{gb} phase form, achieving the balance between weld strength, plasticity and toughness. The width of the lath α phase of the heat-treated weld increases significantly compared with that of α' martensite of the as-welded weld. In addition, dislocation density is reduced greatly in the weld after heat treatment.

2) In the as-welded joint, the proportion of large angle grain boundaries with misorientation between grains in the weld zone greater than 15° accounts for 83.78%, which is about 90.21% in the heat-treated welded joint. The as-welded weld is mainly composed of α' martensite, with a small amount of extremely weak multi-angle α phase diffraction peak. In the heat-treated weld, the central angle position of α phase diffraction peak is consistent with α' martensite in the as-welded weld, with a sharp β phase diffraction peak observed.

3) The microhardness of the two groups of welded joints ranks as weld zone＞heat affected zone＞base metal. The hardness values of the corresponding areas of the two groups of welded joints are slightly different. The overall microhardness value of the heat-treated joint is lower than that of the as-welded joint. When the tensile stress is loaded to 928 and 923 MPa, fracture occurs at the base metal and the weld, respectively. The elongation after fracture and impact properties at room temperature of the heat-treated welded joint are greater than those of the as-welded joint and base metal.

References

1 Long W M, Liu D S, Wu A P *et al. Diamond and Related Materials*[J], 2020, 110: 108 085

2 Long W M, Zhang G X, Zhang Q K. *Scripta Materialia*[J], 2016, 110: 41

3 Zhong Mingjun, Wang Kelu, Lu Shiqiang *et al. Rare Metal*

Materials and Engineering[J], 2021, 50(6): 2149 (in Chinese)
4 Peng Meiqi, Cheng Xingwang, Zheng Chao *et al*. *Rare Metal Materials and Engineering*[J], 2017, 46(7): 1843 (in Chinese)
5 Fang N W, Guo E J, Xu K *et al*. *Materials Research Express*[J], 2021, 8: 56 507
6 Fang N W, Guo E J, Huang R S *et al*. *Materials Research Express*[J], 2021, 8: 16 511
7 Sun W J, Wang S L, Wu M *et al*. *Materials Science and Engineering A*[J], 2021, 824(8): 141 811
8 Zhang C L, Bao X Y, Hao M Y *et al*. *Nature Communications*[J], 2022, 13: 5966
9 Yu W X, Hou S S, Lv Y F *et al*. *Vacuum*[J], 2020, 204: 111 362
10 Lei Z L, Chen Y, Ma S C *et al*. *Materials Science and Engineering A*[J], 2020, 797(21): 140 083
11 Guo Y N, Jung T, Chiu Y L *et al*. *Materials Science and Engineering A*[J], 2013, 562(1): 17
12 Wu C, Zhan M. *Transactions of Nonferrous Metals Society of China*[J], 2019, 29: 997
13 Meng L, Kitashima T, Tsuchiyama T *et al*. *Materials Science and Engineering A*[J], 2020, 771(13): 138 640
14 Sun Z G, Chen G Q, Fu X S *et al*. *Acta Metallurgica Sinica*[J], 2010, 23(5): 357
15 Zuo J H, Wang Z G, Han E H. *Materials Science and Engineering A*[J], 2008, 473(1): 147
16 Castany P, Pettinari-Sturmel F, Crestou J. *Acta Materialia*[J], 2007, 55(18): 6284
17 Lei L, Zhao Q Y, Wu C *et al*. *Journal of Materials Science & Technology*[J], 2022, 99(10): 101
18 Zafari A, Lui E W C, Li M *et al*. *Journal of Materials Science & Technology*[J], 2022, 105(10): 131
19 Zhang L G, Tang J L, Wang Z Y *et al*. *Rare Metals*[J], 2021, 40(8): 2099
20 Pan X L, He W F, Cai Z B *et al*. *Chinese Journal of Aeronautics*[J], 2022, 35(4): 521
21 Quaz M M, Fazal M A, Haseeb A S M A *et al*. *Journal of Rare Earths*[J], 2016, 34(6): 549
22 Prashanth K G, Damodaram R, Maity T *et al*. *Materials Science and Engineering A*[J], 2017, 704(17): 66
23 Sun Q J, Zhou J W, Peng J H *et al*. *Rare Metal Materials and Engineering*[J], 2022, 53(3): 843
24 Ito Y, Murakami S, Tsuji N. *Metallurgical and Materials Transactions A* [J], 2017, 48: 4237
25 Li H, Yang C, Sun L X *et al*. *Materials Letters*[J], 2017, 187(15): 4
26 Sun L B, Wang M Q, Huang L J *et al*. *Materials*[J], 2023, 16(4): 1509
27 Wang M Q, Fang N W, Sun L B *et al*. *Metals*[J], 2023, 13(2): 369
28 Derakhshandeh A, Shahmir H, Nili-Ahmadabadi M. *Journal of Materials Research*[J], 2018, 33: 3809
29 Jones N G, Dashwood R J, Jackson M *et al*. *Acta Materialia*[J], 2009, 57(13): 3830
30 Zhang H, Zhang J Y, Hou J P *et al*. *Acta Materialia*[J], 2022, 241: 118 411
31 Li Yaqiang, Liu Jianhua, Zheng Zhenqiang *et al*. *Acta Metallurgica Sinica*[J], 2020, 56(10): 1335 (in Chinese)
32 Mehdi B, Badj R, Ji V *et al*. *Acta Metallurgica Sinica*[J], 2021, 34(7): 997
33 Chen J, Zhao Y Q, Zeng W D. *Transactions of Nonferrous Metals Society of China*[J], 2007, 17: 93

热处理对钛合金激光填药芯焊丝焊接接头组织和性能的影响

徐　锴[1]，王铭秋[2]，方乃文[1]，武鹏博[1]，黄瑞生[1]，孙徕博[1]，李　伟[3]，王星星[4]，周珍珍[1]，李　帅[4]，张天理[5]

(1. 中国机械总院集团哈尔滨焊接研究所有限公司，黑龙江 哈尔滨 150028)

(2. 上海中巽科技股份有限公司，上海 200120)

(3. 北京金威焊材有限公司，天津 301906)

(4. 华北水利水电大学 河南省高效特种绿色焊接国际联合实验室，河南 郑州 450045)

(5. 上海工程技术大学 材料科学与工程学院，上海 201620)

摘　要：通过激光填丝焊接方法并采用自主开发设计的钛合金药芯焊丝，进行TC4钛合金板的焊接，对获得的焊接接头进行920 ℃/1 h+650 ℃/2 h固溶时效处理，并与焊态焊接接头的组织性能进行对比分析。结果表明：热处理态焊接接头焊缝由α_p相、α_s相集束、α_{gb}相典型的三态组织及点状分布的残留β相构成，未见焊态焊缝中的α'马氏体组织，使焊缝的强度-塑性-韧性得以兼顾；热处理态焊接接头强度降低但延伸率和室温冲击韧性增加；热处理态焊接接头拉伸断口由大量撕裂唇包围，韧窝深且均匀，呈微孔聚合韧性断裂。焊态焊接接头中焊缝区晶粒间的取向差大于15°的大角度晶界占比约83.78%；热处理态焊接接头焊缝中晶粒间的取向差大于15°的大角度晶界占比约为90.21%；通过XRD测试，发现焊态焊缝中主要由α'马氏体组成，还有少量极弱的多角度α相衍射峰，而热处理态焊缝中α相衍射峰中心角度位置与焊态焊缝中α'马氏体一致，另外还发现了较为尖锐的β相（110）衍射峰。

关键词：钛合金；激光填丝焊；热处理；组织性能

作者简介：徐　锴，男，1973年生，研究员，中国机械总院集团哈尔滨焊接研究所有限公司，黑龙江 哈尔滨 150028，电话：0451-86333949，E-mail：xkwelding@163.com